JCTC Journal of Chemical Theory and Computation

# Melting-like Transition in a Ternary Alkali Nanoalloy: $Li_{13}Na_{30}Cs_{12}$

Andrés Aguado* and José M. López

*Departamento de Física Teórica, Universidad de Valladolid, Valladolid 47011, Spain*

Received November 9, 2004

**Abstract:** A theoretical analysis of the equilibrium geometry and thermal behavior of the ternary $Li_{13}Na_{30}Cs_{12}$ alkali nanoalloy is presented. The calculations are based on the orbital-free approach to density functional theory and the classical Newtonian equations to deal with the electronic and atomic subsystems, respectively. An onion-like polyicosahedral structure is found to have the lowest energy, with a core shell formed by Li atoms and an external (incomplete) surface shell formed by Cs atoms, the remaining Na atoms forming an intermediate shell. In a narrow range of 10 meV/atom above the ground-state energy, we identify several other isomers, with varying compositional and structural disorder, but all of them based on a polyicosahedral growing pattern. The most important result extracted from an analysis of thermal properties is that diffusion of Cs atoms at the surface starts at ≈140 K, which is 50 K above typical surface melting temperatures of homogeneous Cs clusters. Thus we conclude that alloying may be useful in enlarging the thermodynamic stability of solid surfaces of clusters beyond its homogeneous limit. As the chemical reactivity of a cluster is known to be highly structure dependent, this observation may be especially relevant to heterogeneous catalysis and related applications. We also analyze the dynamical melting behavior of one of the higher-energy isomers and compare it to that of the ground-state structure.

## I. Introduction

Metal nanoparticles have been known for some time to exhibit enhanced catalytic activity as compared to the bulk phase[1] as well as other chemical and physical "anomalies". By analogy with the bulk situation, it may be expected that the properties of nanoalloys will strongly depend on the segregation/mixing tendencies and geometric structure.

Heterogeneous clusters show a much richer structure in their isomer energy spectra than homogeneous clusters. Following López et al.[2] and Jellinek et al.[3] we will indistinctly use the terms permutational isomer and homotop to designate the isomers obtained from a given topological structure by a permutation of atomic sites. In a homogeneous cluster, such a permutation does not lead to a new isomer. In a nanoalloy, on the contrary, those permutations involving exchanges between atoms of different species will result in a different isomer. Similar to what is found in bulk alloys, the local structure is not exactly the same for different homotops, due to structural relaxations induced by differences in size, bonding, etc., of the atomic species involved. In the case of ternary nanoalloys, the number of homotops increases with the number of atoms $N$ as $3^N$. The different atomic volumes, bond strengths and surface tensions of the species involved will conjointly determine the structure of the lowest-energy isomer and its thermal properties for each composition.[4−6]

Most of the theoretical work on heterogeneous metal clusters has been devoted to structural properties. López et al.[7] studied the segregation properties of Na−Cs and Na−Li nanoalloys of several compositions through static calculations. Similar studies were carried out by Bol et al.[8] on binary Na−K and ternary Na−K−Cs clusters. Ab initio calculations, like those of Deshpande et al.[9] on Na−Li, Joshi and Kanhere[10] on Li−Sn and Chacko et al.[11] on Al−Li clusters, are restricted to small sizes, while consideration of structural

* Corresponding author phone: 00 +34 983 423147; e-mail: aguado@metodos.fam.cie.uva.es.

10.1021/ct049892+ CCC: $30.25 
Published on Web 02/03/2005

preferences in larger bimetallic clusters is usually performed by modeling with phenomenological potentials.[12,13] There are also a few molecular dynamics (MD) simulations on bimetallic clusters which consider their freezing[14] and melting[2,10,15,16] transitions and the influence of temperature on segregation.[17] Very recently, Aguado et al.[4−6] have performed MD simulations of melting in the impurity-doped alkali clusters $A_1Na_{54}$, with A=Li, K, Rb and Cs, and in the binary nanoalloys $Na_{43}Cs_{12}$, $Li_{13}Na_{42}$ and $Na_{13}Cs_{42}$. In this paper, we report the results of extensive MD simulations of the melting-like transition in the ternary $Li_{13}Na_{30}Cs_{12}$ nanoalloy. Although clusters composed only of alkali elements are not especially interesting for specific applications, homogeneous alkali clusters have been thoroughly studied in the past because they are simple metallic systems amenable to both experimentation and computer modeling. They have represented an ideal test-bed for the development of theoretical and experimental methods in cluster physics, and consideration of their properties has helped to clarify very interesting issues such as the evolution of structural, dynamic (thermal) and electronic properties from the atomic to the bulk limit or the discovery of so-called magic numbers. Alkali clusters are thus very important from a fundamental point of view. While it is true that studies on binary and ternary alkali nanoalloys are still scarce, they are expected to play a similar role, contributing to the general understanding of cluster properties specific to multicomponent systems, which could be qualitatively shared by more complex metallic nanoalloys. It is within this wider perspective that consideration of the thermal properties of $Li_{13}Na_{30}Cs_{12}$ is pertinent. We will show that the ground-state structure of $Li_{13}Na_{30}Cs_{12}$, as those of $Li_{13}Na_{42}$ and $Na_{13}Cs_{42}$,[6] is based on core−shell polyicosahedral growing. The different atomic species are distributed in onion-like radial shells, whose radii increase with decreasing surface tension. Contrary to what we found in $Li_{13}Na_{42}$ and $Na_{13}Cs_{42}$, however, the surface of $Li_{13}Na_{30}Cs_{12}$ remains solid up to temperatures which are significantly higher than typical surface melting temperatures of homogeneous Cs clusters.[18] We thus point out the possibility of enlarging the thermal stability range of solid surfaces of clusters by alloying, an observation relevant to applied fields such as heterogeneous catalysis.

The rest of the paper is structured as follows: section II presents a brief summary of our theoretical method, a full account of which can be found in our recent publications.[5] Section III describes our (necessarily approximate) strategy to locate minimum-energy isomers and an extensive analysis of the MD simulations of cluster melting. Finally, section IV offers some concluding remarks.

## II. Theory

For a given spatial configuration of atoms, we evaluate the energy of the cluster and the force acting on each atom by employing density functional theory (DFT) in its Hohenberg−Kohn (HK)[19] representation where the valence electron density stands as the basic variable, thus avoiding employment of auxiliary one-particle orbitals as in its Kohn−Sham (KS)[20] representation. The details of our implementation of this so-called orbital-free DFT scheme have been described in previous work,[4,5,21−23] so we just present briefly the main technical issues. The electronic kinetic energy functional of the electron density is approximated by the gradient expansion around the homogeneous limit through second order.[19,24−26] This means that we keep the local Thomas-Fermi term and the lowest order density gradient correction. The local density approximation is used for exchange and correlation.[27,28] The ionic field acting on the electrons is represented by the local pseudopotential of Fiolhais et al.[29] We have shown in recent publications,[4,5] by explicit comparison of HK- and KS-DFT calculations, that the orbital-free level of theory is adequate to study alkali clusters. This conclusion may not apply to more complex metallic elements, for which an extension either of the electronic kinetic energy functional or the local pseudopotential might be needed.

The cluster under study is placed in a unit cell of a cubic superlattice with edge 62 au and the set of plane waves periodic in that superlattice, up to an energy cutoff of 20 Ryd, is used as a basis set to expand the valence electron density. Following Car and Parrinello,[30] the coefficients of that expansion are regarded as generalized coordinates of a set of fictitious classical particles, and the corresponding Lagrange equations of motion for the electron density distribution are solved in order to determine the optimal electron density for each atomic configuration, as described in ref 5. Forces on atoms are then evaluated by using Hellmann−Feynman's theorem. Thus the dynamics of ions is not Car-Parrinello but Born−Oppenheimer. Fourier transforms are calculated on a $144 \times 144 \times 144$ mesh. The equations of motion are integrated using the Verlet algorithm[31] for both electrons and ions, with time steps of $1 \times 10^{-4}$ atu and $3 \times 10^{-3}$ atu for the electronic and ionic motions, respectively. These choices resulted in a conservation of the total energy better than 0.1%. Several MD runs at different constant energies were performed in order to obtain the caloric curve for each cluster. Previous to each constant-energy run, isokinetic thermalization runs were performed to fix the average value of the temperature. The total simulation time was at least 100 ps for each run at constant energy, but for those energies close to the melting-like transition, some runs longer than 200 ps were performed. The total simulated time for each isomer was close to 2 ns.

The theoretical indicators employed to locate the melting-like transition are as follows: (a) the caloric and specific heat curves as a function of the internal cluster temperature, which is defined through the equipartition theorem for the ionic kinetic energy; (b) the root-mean-squared bond-length fluctuation parameter $\delta$; (c) the diffusion coefficient, obtained from the long time behavior of the mean square displacement; (d) short-time averages of the "atomic equivalence indexes"[32]

$$\sigma_i(t) = \sum_j |\vec{R}_i(t) - \vec{R}_j(t)| \qquad (1)$$

where $\vec{R}_i(t)$ gives the position of atom $i$. These indexes take different values for geometrically inequivalent atoms, and thus are very useful indicators of isomerization and/or

melting transitions; (e) the microcanonical average of the atomic distribution function, defined by

$$dN_{at}(r) = g(r)dr \quad (2)$$

where $dN_{at}(r)$ is the number of atoms at distances from the center of mass between $r$ and $r + dr$. By including just the number of atoms of a given species in the previous expression, we may obtain the partial contributions of each atomic type to the total $g(r)$. Explicit expressions for the rest of indicators can be found in previous publications.[4,5,21−23]

## III. Results

**A. Lowest Energy Isomers.** We have not tried to extensively sample the energy landscape of $Li_{13}Na_{30}Cs_{12}$ by using global optimization techniques such as genetic[12,33] or basin hopping[34] algorithms, as this is a prohibitive task for the energy model we are employing. Instead, we have adopted an approximate sampling scheme, based on dynamical simulated annealing runs and the direct generation of physically motivated structures. This procedure will lead to isomers which are at least reasonably close to the real ground-state structure. Specifically, simulated annealing runs were performed starting from a liquid cluster equilibrated at 200 K, at a cooling rate of 0.2 K/ps, which means a simulation length of 1 ns takes the cluster to 0 K. In practice, we rather stopped the annealing simulation at 5 K and then performed a conjugate gradients optimization of the resulting structure. We also considered isomers constructed by hand with icosahedral, decahedral and cuboctahedral symmetries, which are between the expected topological structures for metal clusters. For each of these isomers, we additionally performed a mild annealing simulation, by heating the cluster to approximately 100 K (in any case, a temperature lower than the melting point) and cooling it down at a rate of 0.4 K/ps. In many cases, this has the effect of locating an isomer of the same symmetry as the original one but with a slightly lower energy.

In the construction of isomers with icosahedral, decahedral and cuboctahedral structures, we took advantage of the knowledge gathered in our previous work on binary Li−Na and Na−Cs clusters.[6] There we found that segregation to the cluster surface of the atomic species with lower surface tension (and, in the case of alkalis, larger atomic radius) was always favored. Thus, we start from an inner core with 13 Li atoms and study what is the best way of adding Na atoms to its surface and then Cs atoms to the resulting structure. Figure 1 shows some of the minimum energy isomers found through this manual procedure as well as from unbiased simulated annealing runs. The isomers obtained from simulated annealing show reduced structural order but competitive energies, and all low-energy isomers are based on polyicosahedral (or anti-Mackay) growing (even though this is less obvious by visual inspection for isomers (c) and (e), for reasons explained below).

In the ground-state isomer as well as in isomers (b) and (d) twenty Na atoms sit on the faces of the $Li_{13}$ icosahedral core and ten Na atoms on top of vertex sites of $Li_{13}$. The differences between these three isomers (and also some higher-energy isomers not explicitly shown) are mostly the

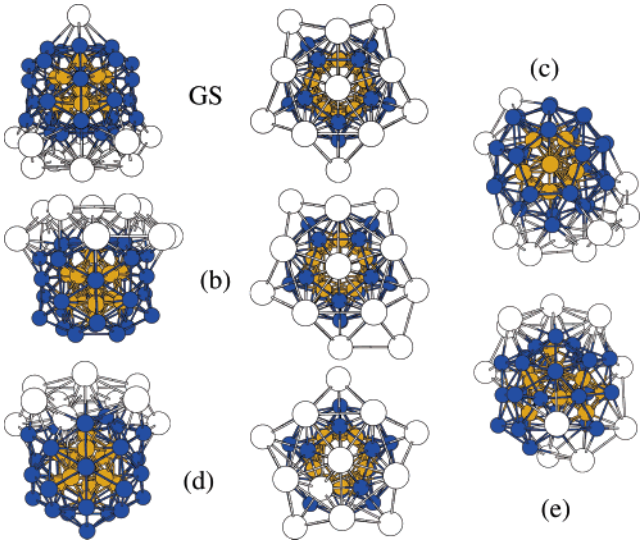


***Figure 1.*** Lowest energy structure (GS) and low-lying isomers of $Li_{13}Na_{30}Cs_{12}$. Side and top views are offered for isomers GS, (b) and (d), which show a higher structural order, while a single view is offered of isomers (c) and (e), which are representative of the results of simulated annealing runs. Small light balls represent Li atoms, medium-size dark balls represent Na atoms, and large white balls represent Cs atoms. The energy differences with respect to the ground-state isomer (GS), in meV/atom, are 0.49 (b), 2.22 (c), 2.34 (d) and 6.7 (e).

allocation of the remaining Cs atoms. In the GS isomer, two of them complete the anti-Mackay 32-atom shell by sitting on top of the uncapped vertex sites of $Li_{13}$, while the others form a single umbrella on top of the $Li_{13}Na_{30}Cs_2$ structure. The lonely Cs atom in the GS isomer moves close to the rest of Cs atoms in isomer (b), so that one of the vertex sites of $Li_{13}$ remains uncapped. In isomer (d), this vertex site is capped by a Na atom, and one of the Cs atoms sits on top of a face position of $Li_{13}$. Isomers (c) and (e) are representative of the kind of isomers found from simulated annealing runs. Isomer (c) contains an icosahedral $Li_{12}Na$ core, which shows that slight mixing of Li and Na species has not a big energy penalty. The core shell of isomer (e) is a $Li_9Na_4$ icosahedron. Due to the larger number of Na atoms in the inner shell, the second shell is formed by a mixture of Li, Na, and also Cs atoms. There are also some Na atoms in the most external surface shell, so mixing is much more pronounced in this isomer. Growing is still strictly polyicosahedral, so that, apart from the outermost surface shell, all isomers in Figure 1 are just homotops of the same inherent structure. The reason that isomers (c) and (e) are more structurally disordered is just the local distortions appearing due to the different atomic species. In fact, we did not find any isomer with a type of growing other than anti-Mackay in any of the simulated annealing runs, which demonstrates that this is really the preferred structural motif when different shells are preferentially formed by alkalis of different size. However, the simulated annealing runs, at least at the cooling rates employed here, are not able to find the optimal compositional order.

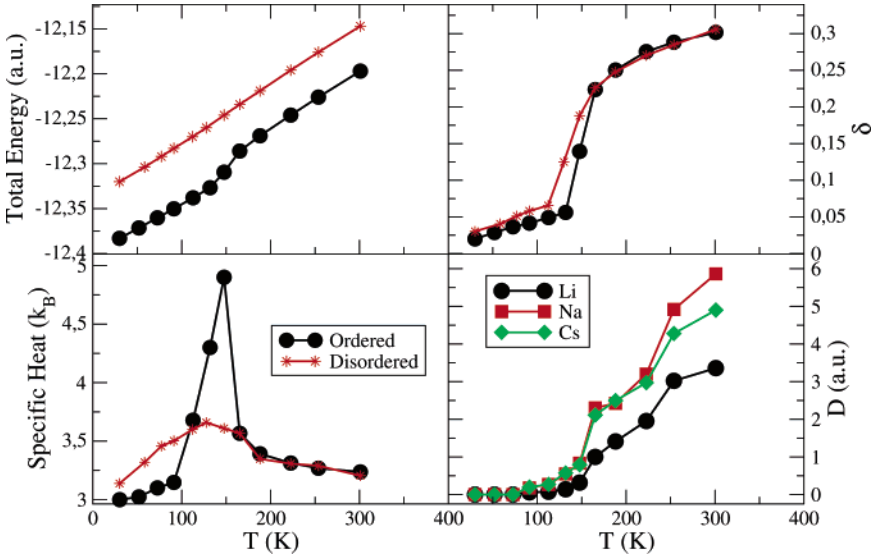


***Figure 2.*** Caloric and specific heat curves (left side) and rms bond length fluctuation and diffusion constants (right side) of $Li_{13}Na_{30}Cs_{12}$, taking the average internal cluster temperature as the independent variable. The diffusion coefficients are shown just for the ground-state isomer, while the rest of indicators are also shown for the isomer (e) in Figure 1. The caloric curve for this last isomer has been vertically displaced for clarity.

Polyicosahedral structures in binary metal clusters have been independently identified by Rossi et al.[13] for the case of noble metals and by Aguado and López[6] for the case of alkali metals. In homogeneous clusters, this growing pattern accumulates a very large strain in the inner 13-atom icosahedron and thus is not usually observed. In a binary AB nanoalloy, on the contrary, the atomic species with the shortest equilibrium interatomic distance and/or higher surface tension (A) may form the inner $A_{13}$ icosahedral core with little or no accumulated strain. At the same time, A−B interatomic distances and packing of B-atoms can both be optimized by anti-Mackay growing because only 20 faces (as opposed to 30 edges) need to be capped. As Rossi et al. point out, particularly stable polyicosahedral structures are expected whenever the differences in surface energies and atomic sizes of the species involved are sufficiently large. In this work, we have shown this to be generalizable to the case of ternary Li−Na−Cs nanoalloys. However, there is an important difference between $Li_{13}Na_{30}Cs_{12}$ and the binary clusters considered in ref 6: as an anti-Mackay overlayer is completed at composition $A_{13}B_{32}$, the 10 Cs atoms forming the outermost shell in $Na_{13}Cs_{42}$ sit on top of an inner Cs shell, and these external Cs atoms do not strictly conform to polyicosahedral order. In $Li_{13}Na_{30}Cs_{12}$, each shell is mostly formed by a different type of atom, which enforces strict polyicosahedral order. We will see that the higher structural order confers the cluster with enhanced thermal stability.

To close this section, we would like to emphasize that the energetic ordering of the isomers presented here is preserved by orbital-based KS-DFT calculations performed with the SIESTA code,[35] under the same approximation for exchange-correlation effects and with core electrons substituted by norm-conserving pseudopotentials[36] in their fully nonlocal form.[37] This is a general result that we have found in all our previous studies on alkali clusters, which shows that the energy landscape generated by the orbital-free technique is realistic for these materials. Binding energies, measuring the energy required to dissociate the cluster into infinitely separated atoms, are usually much less accurate than energy differences between isomers,[21] because the present orbital-free technique is not well suited to the description of an isolated atom. This means that the evaporation limit cannot be properly described by our method, but the solid-to-liquid transition of clusters of these sizes can be safely addressed. Average interatomic distances are of the order of 1−2% longer than corresponding ab initio values, so melting points may be somewhat underestimated compared to Kohn−Sham results. We are presently considering the possibility that an adaptation of the local pseudopotentials (generated in a bulk environment) to a cluster environment may help to solve this problem, providing results in even better agreement with KS calculations. Finally, the ground-state structure shown in Figure 1 is stable against mild annealing from a temperature of 100 K, and no isomers with significantly lower energy were found in the heating runs reported in the next sections. Thus, the structure proposed is really a good candidate for the minimum energy structure.

**B. Melting-like Transition.** In this section, we analyze by constant-energy MD simulations the melting process for two $Li_{13}Na_{30}Cs_{12}$ isomers, namely the ground state and isomer (e). As it is well-known, the melting transition may be intrinsically isomer-dependent in these simulations if several basins in the energy landscape are separated by high energy barriers. We thus explicitly consider the melting transition of isomer (e) in order to have an estimate for the effect of compositional and structural order on melting properties.

Figure 2 shows the caloric curve as well as the temperature evolution of the specific heat, rms bond length fluctuation and diffusion constants. The most noteworthy result from this figure is that the caloric and specific heat curves of both isomers are very different, even though the location of the melting point itself, given the difficulty of obtaining con-

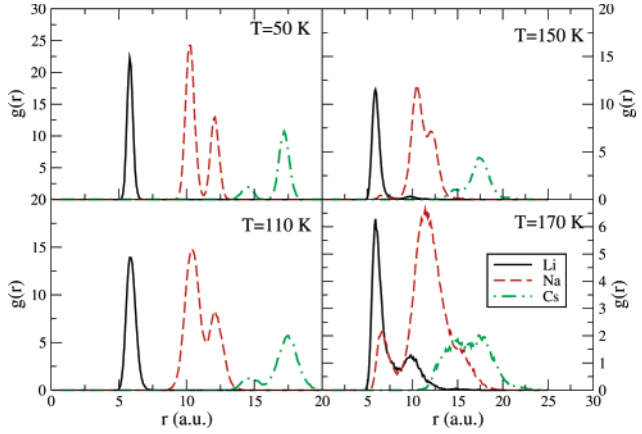


***Figure 3.*** Partial contribution of each atomic species to the time averaged radial atomic density distribution of the ground-state isomer of $Li_{13}Na_{30}Cs_{12}$, at some representative temperatures. The $g(r)$ distributions are calculated with respect to the innermost Li of the 13-atom icosahedral core for both isomers. Due to the nonspherical shape of the cluster, employing the center of mass (as was done in our previous publications) does not permit to distinguish the atomic shell structure. At $T = 170$ K (lower-right panel), that innermost Li atom also interchanges its position with other Li atoms. In this case, the $g(r)$ at each time step was evaluated with respect to that Li atom which instantaneously occupies the innermost position.

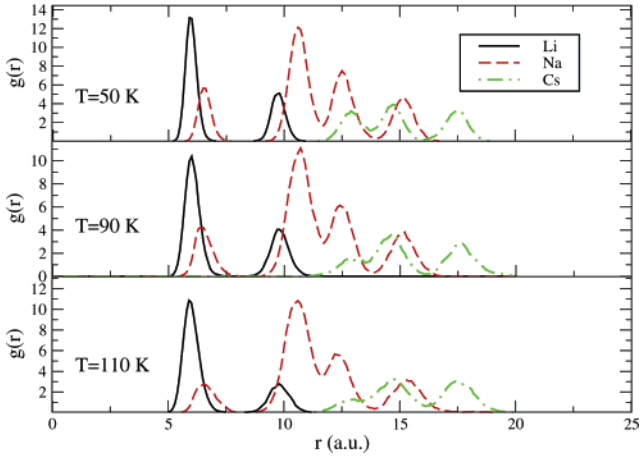


***Figure 4.*** Same as Figure 3, but for isomer (e) in Figure 1.

verged statistical averages in the transition region, is about the same in both cases. It is important to remark here that in a fully ergodic simulation all isomers compatible with a given constant energy $E$ are visited, and thus the differences in specific heat curves can only reflect the nonergodicity of MD simulations. Put in different terms, the averages shown in Figure 2 are not strictly thermodynamic. Nevertheless, what is really important is to understand which situation (if any) is realized in a given experimental determination of melting properties. In the calorimetric experiments of Haberland's group, for example,[38] mass-selected clusters are first thermalized by direct contact with a macroscopic heat bath and then transferred to a high-vacuum region, where each cluster evolves at constant energy. The lower the temperature of the heat bath, the narrower the energy distribution of isomers obtained in the thermalization step, and thus the obtained caloric curve is expected to approach that calculated from constant-energy MD simulations of melting of the GS isomer alone. On the contrary, higher initial temperatures will lead to experimental caloric curves which should be compared to some weighted average of those obtained from constant-energy MD simulations of melting of several isomers.

All indicators in Figure 2 predict that $Li_{13}Na_{30}Cs_{12}$ melts at an approximate temperature $T_m$ of 140 K. The main difference between both isomers is that the GS isomer is much more resistant to premelting (isomerization) effects, as evidenced by the different values of the specific heat at low temperatures. To better understand the origin of the differences, Figures 3 and 4 show partial contributions to the radial atomic density distributions of each isomer, and Figures 5 and 6 short-time averages of the atomic equivalence indexes, for several average temperatures. Regarding the GS isomer, the partial contributions to $g(r)$ hardly overlap up to the melting point. At $T$=150 K (slightly above $T_m$), we observe the first interchange between Li and Na atoms, which means that the basin of isomer (c) starts to be visited. At a higher temperature of 170 K, Li−Na mixing is enhanced, and some overlap of Na and Cs contributions is also appreciated at the surface. In this region, isomers similar to (e) are routinely visited. Figure 4 shows that the cooling rate computationally affordable in the simulated annealing runs is still too fast to find the correct distribution of atoms within the polyicosahedral shells. In fact, as far as the partial contributions to $g(r)$ are concerned, the structure of isomer (e) is very similar to an average liquid structure. Thus, the distribution of atoms in shells does not appreciably change upon heating. Figures 5a and 6 show that radial structural order is much higher in the GS structure, as the several $\sigma$ lines are separated by well defined gaps, while just a loose differentiation between core and surface shells is apparent for isomer (e). Nevertheless, both isomers have approximately the same volume, despite the strong local relaxations in isomer (e). As stated in the previous section, this important difference in the atomic equivalence indexes is just driven by local structural relaxations, as both isomers are homotops of the same topological isomer. Figure 5b shows that at a temperature as high as 130 K, the GS isomer is still a hot solid, while structural isomerizations are observed in isomer (e) even at 50 K (Figure 6), implying that we are in a region of configurational space with a high density of isomeric states, which are separated by sufficiently low barriers (this is a feature typical of the energy landscapes of amorphouslike materials). Figure 4 shows that these low-T isomerizations try to drive the cluster structure toward that of the GS isomer: for example, Na−Cs mixing is reduced upon heating to 90 K, and the same is true of Li−Na mixing at 110 K (note the heights of the several $g(r)$ peaks). This observation suggests that a much slower cooling rate in simulated annealing runs would result in better approximations to the GS structure, as expected. For the GS isomer, the liquid structure is not yet well developed even at 150 K (Figure 5c). For example, the innermost Li-atom stays vibrating about its equilibrium position for the whole simulation, which is close to 200 ps long. The cluster is clearly liquidlike at 170

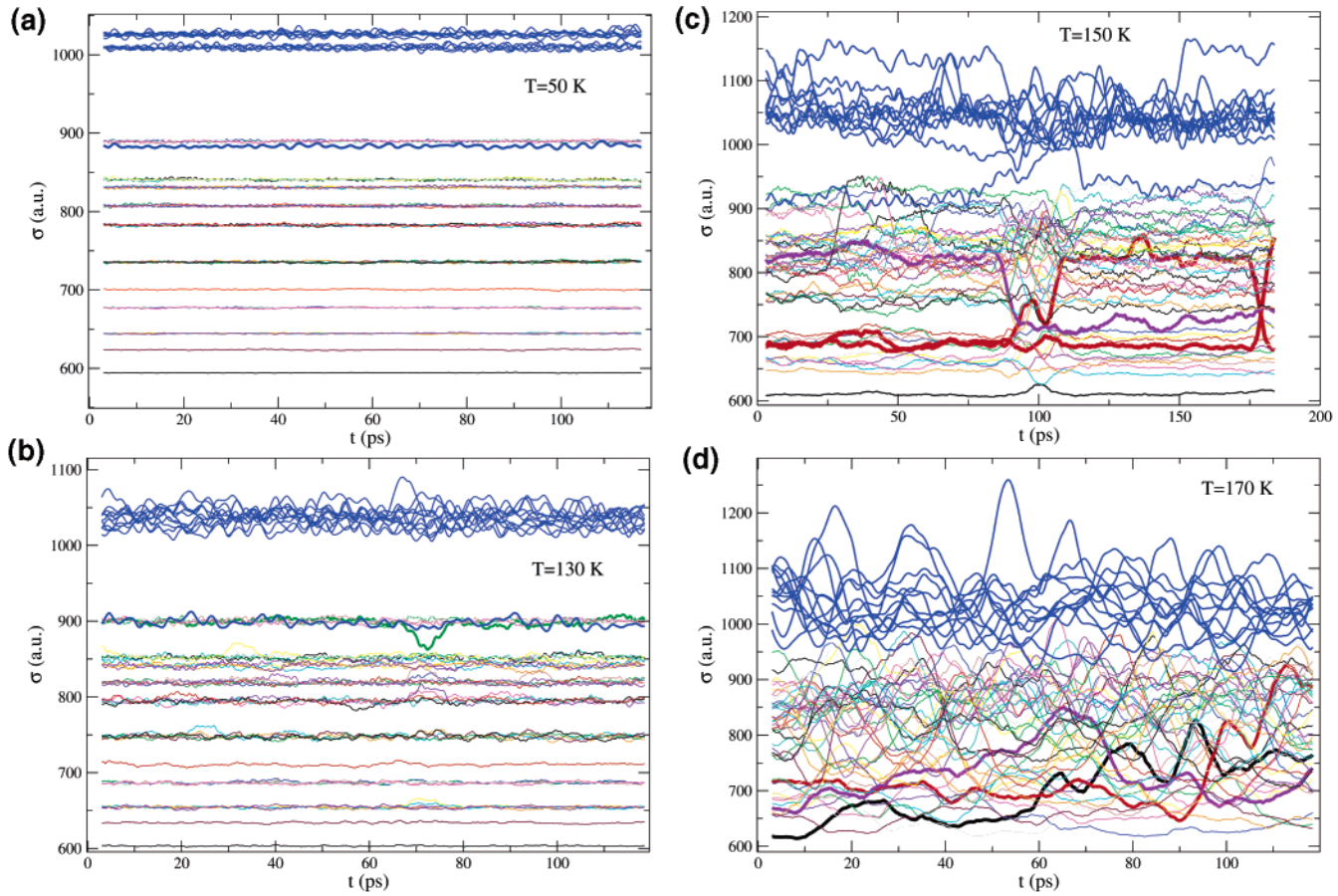


***Figure 5.*** Time evolution of atomic equivalence indexes of the ground-state isomer of $Li_{13}Na_{30}Cs_{12}$, averaged over time intervals of 1000 steps, at four representative temperatures. $\sigma$ curves corresponding to Cs atoms as well as those of other species involved in isomerization transitions and diffusion are represented by bold lines in order to help visualization.

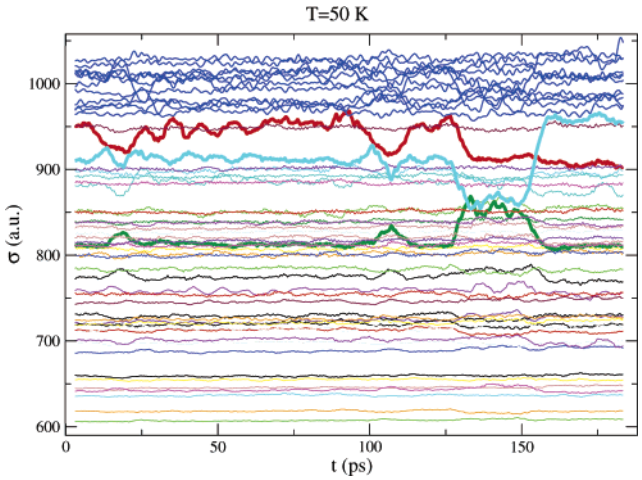


***Figure 6.*** Same as Figure 5, but for the disordered $Li_{13}Na_{30}Cs_{12}$ isomer at 50 K.

K, however (Figure 5d), in correspondence with the steplike increase in diffusion appreciated in Figure 2.

## IV. Summary and Discussion

In this paper, orbital-free DFT molecular dynamics simulations have been employed in order to analyze the structure and melting mechanism in a ternary alkali nanoalloy, namely $Li_{13}Na_{30}Cs_{12}$. The orbital-free DFT method is chosen because it provides a good compromise between statistical accuracy and realistic interatomic forces.

The lowest-energy structure is dictated by the relief of core strain and the tendency of surface bonds to contract. When the atomic species have significantly different sizes and surface energies, these "rules" lead to polyicosahedral clusters (with segregation of the lower surface energy component to the cluster surface) in a natural way. No significant strain is accumulated in the core shell of these structures as the smaller size species has a shorter equilibrium bond distance. At the same time, optimal distances for the surface bonds may be obtained by growing of the large size species on the faces of the inner icosahedron (growing on edge sites would result in surface bonds which are too short). Anti-Mackay growing is so energetically favorable that none of the simulated annealing runs has found even one isomer with a different symmetry. Simulated annealing is nevertheless not able to find the correct compositional order for computationally affordable cooling rates.

The most important finding is that the melting transition in the GS isomer of $Li_{13}Na_{30}Cs_{12}$ is located at a temperature which is approximately 50 K higher than typical surface melting temperatures of pure Cs clusters obtained with the same method.[18] On the contrary, premelting effects are noticeable for $Li_{13}Na_{42}$ and $Na_{13}Cs_{42}$ at considerably lower temperatures as compared to homogeneous Na and Cs

clusters, respectively.[6] The main difference between both cases is that the GS structure of $Li_{13}Na_{30}Cs_{12}$ is strictly polyicosahedral, with atoms of different species mostly occupying different radial shells; on the contrary, the outermost surface atoms of $Li_{13}Na_{42}$ and $Na_{13}Cs_{42}$ grow on top of an inner shell formed by ions of the same type, and the growing pattern is not polyicosahedral in that external region. It thus seems that strict polyicosahedral packing of approximately spherical layers, each formed by alkali atoms of different types lead to enhanced thermal stability of the solid phase. The net result is that diffusion of surface Cs atoms grown on a Cs "substrate" is easier than the corresponding diffusion on a substrate formed by alkali atoms of smaller size. In the future, we plan to undertake MD simulations of a larger number of binary and ternary alkali clusters with geometrically compact structures in order to determine more unambiguously the physical reason for this melting temperature increase. It is important to get such a sound understanding because it might be used to build material surfaces which remain solid up to significantly higher temperatures than expected.

We have also explicitly simulated the thermal behavior of a low-lying isomer of the same cluster, obtained from simulated annealing runs. This isomer also has a perfect polyicosahedral structure, but each radial shell is formed by a mixture of atoms of different types. As a result of this partial compositional disorder, local structural distortions appear in much the same way as in a bulk alloy, and the resulting distribution of atoms in radial shells is reminiscent of that expected for an amorphous-like structure. Premelting effects, in this case realized as structural isomerizations, are then observed even at very low temperatures. This seems to be the most general behavior of alkali nanoalloys, while the enhanced melting temperatures are observed only in structures with high topological (polyicosahedral in the case at hand) and compositional orders.

Finally, we have emphasized that, even though the premelting effects are highly isomer-dependent, the homogeneous melting temperature itself is the same for both isomers within the statistical accuracy of our simulations. The caloric curves are different for both isomers simply because constant-energy MD simulations, started from a given isomer, can only sample the region of phase space which is dynamically accessible to that isomer. At low energies, this represents an essential loss of ergodicity (one which cannot be restored just by increasing the length of the simulation) if basins of different isomers are separated by high energy barriers. We stress this point because we believe that our MD runs for the GS structure are long enough as to obtain nearly-converged results with respect to simulation time, except possibly for the transition region. The simulations presented for the low-lying isomer, where relatively *high energies* (and, correspondingly, phase-space regions with high density of states) are sampled at *low temperatures*, might suffer more from convergence problems at the lowest temperatures. In any case, we have indicated that care must be exercised in comparing the MD results to a hypothetical experimental determination of the caloric curve.

**Acknowledgment.** This work was supported by Junta de Castilla y León (Project VA073/02) and DGES (Project MAT2002-04393-C02-01). Thanks are due to J. M. Soler and his team for providing us with a copy of the SIESTA code and to M. J. López for helping us with the construction of icosahedral, cuboctahedral and decahedral geometries. A.A. also acknowledges financial support from the Spanish Ministry of Science and Technology, under the Ramón y Cajal program.

## References

(1) Haruta, M. *Catal. Today* **1997**, *36*, 153−166.

(2) López, M. J.; Marcos, P. A.; Alonso, J. A. *J. Chem. Phys.* **1996**, *104*, 1056−1066.

(3) Jellinek, J.; Krissinel, E. B. *Chem. Phys. Lett.* **1996**, *258*, 283−292. Krissinel, E. B.; Jellinek, J. *Chem. Phys. Lett.* **1997**, *272*, 301−312.

(4) Aguado, A.; González, L. E.; López, J. M. *J. Phys. Chem. B* **2004**, *108*, 11722−11731; Aguado, A.; Núñez, S.; López, J. M. *Comput. Mater. Sci.* in press.

(5) Aguado, A.; González, D. J.; González, L. E.; López, J. M. in *Progress in Chemical Physics Research*; Columbus, F., Ed.; Nova Science Publishers: New York, 2005, in press.

(6) Aguado, A.; López, J. M. *Phys. Rev. B* in press.

(7) López, M. J.; Mañanes, A.; Alonso, J. A.; Íñiguez, M. P. *Z. Phys. D* **1989**, *12*, 237−239; López, M. J.; Íñiguez, M. P.; Alonso, J. A. *Phys. Rev. B* **1990**, *41*, 5636−5642; Mañanes, A.; Íñiguez, M. P.; López, M. J.; Alonso, J. A. *Phys. Rev. B* **1990**, *42*, 5000−5008.

(8) Bol, A.; Alonso, J. A.; López, J. M.; Mañanes, A. *Z. Phys. D* **1994**, *30*, 349−356. Bol, A.; Martín, G.; López, J. M.; Alonso, J. A. *Z. Phys. D* **1993**, *28*, 311−319.

(9) Deshpande, M. D.; Kanhere, D. G.; Panat, P. V.; Vasiliev, I.; Martin, R. M. *Phys. Rev. A* **2002**, *65*, 053204(1)−053204-(5). Deshpande, M. D.; Kanhere, D. G.; Vasiliev, I.; Martin, R. M. *Phys. Rev. A* **2002**, *65*, 033202(1)-033202(6).

(10) Joshi, K.; Kanhere, D. G. *Phys. Rev. A* **2002**, *65*, 043203-(1)−043203(7).

(11) Chacko, S.; Kanhere, D. G.; Paranjape, V. V. *Phys. Rev. A* **2004**, *70*, 023204(1)−023204(9).

(12) Darby, S.; Mortimer-Jones, T. V.; Johnston, R. L.; Roberts, C. *J. Chem. Phys.* **2002**, *116*, 1536−1550. Bailey, M. S.; Wilson, N. T.; Roberts, C.; Johnston, R. L. *Eur. Phys. J. D* **2003**, *25*, 41−55.

(13) Rossi, G.; Rapallo, A.; Mottet, C.; Fortunelli, A.; Baletto, F.; Ferrando, R. *Phys. Rev. Lett.* **2004**, *93*, 105503(1)−105503(4).

(14) Chushak, Y. G.; Bartell, L. S. *J. Phys. Chem. B* **2003**, *107*, 3747−3751.

(15) Huang, S.; Balbuena, P. B. *J. Phys. Chem. B* **2002**, *106*, 7225−7236.

(16) Joshi, K.; Kanhere, D. G. *J. Chem. Phys.* **2003**, *119*, 12301−12307.

(17) Mainardi, D. S.; Balbuena, P. B. *Int. J. Quantum Chem.* **2001**, *85*, 580−591.

(18) Aguado, A. *Phys. Rev. B* **2001**, *63*, 115404(1)−115404(9).

(19) Hohenberg, P.; Kohn, W. *Phys. Rev.* **1964**, *136*, B864−B871.

(20) Kohn, W.; Sham, L. J. *Phys. Rev.* **1965**, *140*, A1133−A1138.

(21) Aguado, A.; López, J. M.; Alonso, J. A.; Stott, M. J. *J. Chem. Phys.* **1999**, *111*, 6026−6035.

(22) Aguado, A.; López, J. M.; Alonso, J. A.; Stott, M. J. *J. Phys. Chem. B* **2001**, *105*, 2386−2392.

(23) Aguado, A.; Molina, L. M.; López, J. M.; Alonso, J. A. *Eur. Phys. J. D* **2001**, *15*, 221−227.

(24) *Theory of the inhomogeneous electron gas*; Lundqvist, S.; March, N. H., Eds.; Plenum Press: New York, 1983.

(25) Yang, W. *Phys. Rev. A* **1986**, *34*, 4575−4585.

(26) Perdew, J. P. *Phys. Lett. A* **1992**, *165*, 79−82.

(27) Perdew, J. P.; Zunger, A. *Phys. Rev. B* **1981**, *23*, 5048−5079.

(28) Ceperley, D. M.; Alder, B. J. *Phys. Rev. Lett.* **1980**, *45*, 566−569.

(29) Fiolhais, C.; Perdew, J. P.; Armster, S. Q.; McLaren, J. M.; Brajczewska, H. *Phys. Rev. B* **1995**, *51*, 14001−14011. Fiolhais, C.; Perdew, J. P.; Armster, S. Q.; McLaren, J. M.; Brajczewska, H. *Phys. Rev. B* **1996**, *53*, 13193−13193.

(30) Car, R.; Parrinello, M. *Phys. Rev. Lett.* **1985**, *55*, 2471−2474. Payne, M. C.; Teter, M. P.; Allan, D. C.; Arias, T. A.; Joannopoulos, J. D. *Rev. Mod. Phys.* **1992**, *64*, 1045−1097.

(31) Verlet, L. *Phys. Rev.* **1967**, *159*, 98−103. Swope, W. C.; Andersen, H. C. *J. Chem. Phys.* **1982**, *76*, 637−649.

(32) Bonacić-Koutecký, V.; Jellinek, J.; Wiechert, M.; Fantucci, P. *J. Chem. Phys.* **1997**, *107*, 6321−6334. Reichardt, D.; Bonacić-Koutecký, V.; Fantucci, P.; Jellinek, J. *Chem. Phys. Lett.* **1997**, *279*, 129−139.

(33) Soler, J. M.; Garzón, I. L.; Joannopoulos, J. D. *Solid State Comm.* **2001**, *117*, 621−625, and references therein.

(34) Doye, J. P. K. *Phys. Rev. B* **2003**, *68*, 195418(1)−195418-(11).

(35) Soler, J. M.; Artacho, E.; Gale, J. D.; Garc×c1a, A.; Junquera, J.; Ordejón, P.; Sánchez-Portal, D. *J. Phys.: Condens. Matter* **2002**, *14*, 2745−2779.

(36) Hamann, D. R.; Schlüter, M.; Chiang, C. *Phys. Rev. Lett.* **1979**, *43*, 1494−1497.

(37) Kleinman, L.; Bylander, D. M. *Phys. Rev. Lett.* **1982**, *48*, 1425−1428.

(38) Schmidt, M.; Kusche, R.; Kronmüller, W.; von Issendorff, B.; Haberland, H. *Phys. Rev. Lett.* **1997**, *79*, 99−102. Schmidt, M.; Kusche, R.; von Issendorff, B.; Haberland, H. *Nature* **1998**, *393*, 238−240. Kusche, R.; Hippler, Th.; Schmidt, M.; von Issendorff, B.; Haberland, H. *Eur. Phys. J. D* **1999**, *9*, 1−6. Schmidt, M.; Haberland, H. *Compt. Rend. Physique* **2002**, *3*, 327−340.

CT049892+